A long term geomagnetic deep sounding analysis from a two-dimensional magnetometer array in Central Italy

C. Di Lorenzo, P. Palangio, A. Zirizzotti and C. Bianchi

Istituto Nazionale di Geofisica e Vulcanologia, Italy

Correspondence to: C. Di Lorenzo (cinzia.dilorenzo@ingv.it)

Abstract

Following the earthquake that hit the city of L'Aquila on the 6th April 2009, a scientific project was proposed with the aim of investigating the Abruzzo area by means of different disciplinary approaches including geological, seismic, and physical studies. Electromagnetic field monitoring in the 0.01-500 mHz frequency band was implemented for the investigation of electromagnetic signals in the Earth's crust. Three measurement stations were installed in a tectonically active with a radius of about ten kilometres. Each site was equipped with a fluxgate magnetometer with a 1 Hz sampling rate. This paper describes a long term geomagnetic deep sounding analysis for each site in order to investigate the dimensionality of the electrical structure of the subsoil in the area involved in the survey.

1 Introduction

Electromagnetic signals produced by tectonic activity span a wide frequency range from DC to HF (Johnston M.J.S., 1997; Molchanov O.A. et al., 1998). ULF electromagnetic phenomena are more likely to be detected from ground observations than signals at higher frequencies because of the greater skin depth. Different mechanisms are thought to generate electromagnetic emissions in response to crustal deformations (changes in magnetization or electrical resistivity of crustal rocks, electric currents generated by fluids flowing in the Earth's crust, charge generation mechanisms) (Johnston M. J. S, 2002; Molchanov O.A. et al., 1995). As they propagate through the terrestrial crust, the waves are attenuated by a factor that depends on the electrical structure of layers traversed. Knowledge of this parameter is

important when studying electromagnetic signals related to tectonic activity. Geomagnetic Deep Sounding (GDS) is one of the most widely used techniques to investigate the vertical distribution of electrical conductivity. This method allows qualitative analysis of lateral discontinuities using only the magnetic measurements from a single site (Banks R.J, 1973). GDS is a passive method based on the inductive response of the Earth's crust and upper mantle to electromagnetic signals originating from magnetospheric and ionospheric currents. Magnetometer array data makes it possible to map conductive structures and study their tectonic implications. (D. Ian Gough, 1989). Simultaneous data from two (Palangio et al., 2009) or more sites (Alabi, 1983) enables a quantitative interpretation. In a way analogous the magnetotelluric method, the gradiometric magnetic approach can be used to estimate apparent resistivity (Hermance, 1995; Schmucker, 1970). This paper presents a GDS analysis for each station in the magnetic network.

2 The network stations

Within the framework of the National "Firb Abruzzo" project, a network of three electromagnetic stations was installed near L'Aquila (central Italy). The stations were set out in an array scaled to match the depth of the sismogenetic zone (10-15 Km). This positioned each station in the near field of sismogenetic sources in the frequency band up to 100 Hz (Meloni et al., 2015). Magnetic data were acquired using a triaxial fluxgate magnetometer (Lemi 18) with a 1 Hz sampling rate, and a triaxial search coil magnetometer (Metronix ADU-07) with a 256 Hz sampling rate. Electric field was measured using two horizontal ADU-07 sensors. Figure 1 shows the array layout of the three stations: Collebrincioni (CLB), Paganica (PGN), and Preturo (PRT). They are located at the vertices of a nearly isosceles triangle on a plane inclined by about 3° to the horizontal. These sites were selected after a magnetic measurement campaign at eight points in the chosen area. A maximum distance between the measuring stations of less than 13 km was chosen on the basis of the structure of the electrical conductivity of the subsoil in the area, evaluated in a previous magnetotelluric study (Palangio et al., 2009). Noise analysis was performed by Principal Component Analysis with Singular Value Decomposition (or the discrete Karhunen-Loève transform) applied to the covariance matrix. This methodology enabled separation of the magnetic signal from the surrounding noise (Clifford G.D., 2005). Figure 2 shows the first eight eigenvalues of the covariance matrix obtained for the PGN station as an example. The first three eigenvalues are

those associated with the principal external natural sources while the last five eigenvalues represent the largest sources of noise. Total magnetic noise is represented in figure 3 and was obtained by the linear combination of the eigenvalues associated with the noise with their relative eigenfunctions at the PGN station. The analysis involved separating the two time segments 03-21 UT (day) and 21-03 UT (night). The root mean square values for each magnetic component in the two time intervals are shown in the figure. The peak intensity during day-time is due to human activities. Despite its low level, the noise is greater than the amplitude of the endogenic signals, requiring the use of high sensitivity measuring instruments, in the order of picoTesla, like search coil magnetometers. However, to discriminate very weak signals from the Earth's interior, a single site measurement is not sufficient and a gradiometric approach is required using simultaneous measurements from the three stations. This technique, which will be published at a later date, makes it possible not only to eliminate the contribution of external natural field signals whose gradient is null across the distance between the measurement stations, but also to discriminate internal signals from external signals by analysing the phase difference of the gradient of magnetic signals (Clark, 2012). The magnetic sensors at the stations were housed in two fiberglass tanks buried at a depth of about 2 meters in order to achieve passive temperature stabilization, eliminate wind induced vibrations, and increase the mechanical stability of the sensors. Solar panels were used to power the system with a linear charge controller to charge the batteries supplying all the instrumentation. All power devices were mounted on an aluminium trellis about 100 meters away from the instrumentation to prevent interference, with all power cables and signal transmissions being "twisted" and shielded for the same reason. The trellis also housed the power supply system and antennas of a GSM-UMTS router for data transmission, connecting the equipment to the Internet through the local telephone network. Figures 4, 5, and 6 show the three sites, and figures 7 and 8 show the search coil magnetic sensors and fluxgate magnetometers. All the sensor are orientated along the geomagnetic reference system H, D, and Z. The CLB station is shown in figure 4 as an example, and more details about the station implementations are available in Di Lorenzo et al. 2016.

3 Geomagnetic Deep Sounding Analysis

At mid latitudes, magnetic field variations on the Earth's surface produced by the electrical currents in the most conductive layer of the ionosphere (altitude ~100 Km) are almost

horizontal and uniform over hundreds of kilometres. The principal source of these currents is a dynamo mechanism due to differential solar heating of the ionospheric plasma which drives a sheet current in the day side hemisphere, which is responsible for the so called 'diurnal variation' (Matsushita S., 1967, 1968). At higher frequencies (ULF band), magnetic signals are produced by an interaction between the solar wind and the Earth's magnetosphere, known as geomagnetic micropulsation. (McPherron et al., 1972). Both these external natural sources are usually employed when sounding the electrical structure of the Earth's crust and upper mantle. The propagation into the Earth of magnetic waves with periods from 1 to 10^5 s is a diffusive process ($\sigma >> \omega\varepsilon$) because the Earth's conductivity varies from 10^{-4} to 10 S/m. According to the expression of the *skin depth*:

$$\delta = \sqrt{\frac{2}{\mu_0 \sigma \omega}} \tag{1}$$

when $\mu_0 = 4\pi \cdot 10^{-7}\ H/m$ is magnetic permeability in a vacuum and σ is the Earth's mean conductivity integrated across the transit layers. Lower frequencies penetrate deeper into the ground. In a simple horizontally stratified structure, the induced currents are also horizontal and would produce a horizontal magnetic field in the case of an infinitely extended conductor. A vertical magnetic component appears in the case of lateral discontinuities due to electrical currents flowing along the boundaries separating regions of different conductivity. This component is therefore defined the 'anomalous' induced field. Using data from a single measurement station, a geomagnetic induction study is reduced to a problem of an 'input-output system' in which the inputs are the horizontal magnetic variations H and D of external origin, and the output is the induced vertical magnetic field Z caused by electrical currents flowing along the discontinuity boundaries. In the frequency domain the relation between the horizontal and vertical magnetic components is expressed by the linear equation:

$$Z(f) = A(f)H(f) + B(f)D(f) + \varepsilon(f) \tag{2}$$

when the last term represents the non inductive component due to the vertical component of external sources (although the horizontal field of external sources is a good approximation, it was not possible to ignore the presence of a small vertical component produced by toroidal currents in the ionosphere). A and B are defined the magnetic transfer functions (TF) and are complex quantities, usually represented as a vector, the *induction arrow* or *tipper* [A B]. Since the solutions of the diffusive problem are related to the electrical structure of the

Earth's subsoil, the magnetic transfer functions provide information about geoelectric dimensionality. For a 1D Earth the solutions that satisfy the problem predict a completely horizontal magnetic field. As a consequence the predicted A and B values would both be null. A vertical magnetic field would appear in a 2D structure, associated to the transverse electric (TE) mode. In this case only the horizontal component perpendicular to the *strike* (the direction along which conductivity is constant) is responsible for the induction. As a consequence only the corresponding coefficient (A or B) will differ from zero. Magnetic transfer function are therefore useful to identify the direction of geoelectric discontinuity. However, this method requires a further step before interpreting the data. This is because the strike direction is usually not known *a priori* and so magnetic measurements are generally made in a general reference system rotated relative to the strike. Methods based on the maximisation of coherence between the horizontal and vertical magnetic fields make it possible to find the strike direction *a posteriori* (G.D. Naidu, 2012). A more immediate analysis independent of the orientation of the measurement system makes use of the combination of A and B as a vector (the tipper/induction arrow) of amplitude and phase defined as:

$$T_{amp}(f) = \sqrt{A^2(f) + B^2(f)} \tag{3a}$$

$$T_{phase}(f) = a\tan(B(f)/A(f)) \tag{3b}$$

The first is rotationally invariant. In a 2D structure the position of the tipper identifies the strike orientation. It is perpendicular to the strike and its magnitude is proportional to the intensity of anomalous currents. In the Wiese (Gubbins, D., Herrero-Bervera E., 2007) convention the tipper arrow points towards the region of lower conductivity or, by adding 180°, the reversed *Parkinson vector* points towards the region of higher conductivity where the anomalous currents are concentrated (HOBBS, 1992). Another rotational invariant is the *tipper skew*. This is a measure of dimensionality or noise for GDS data, its expression being related to the determinant of the TF tensor as:

$$S(f) = \frac{2}{T}\begin{vmatrix} A_{re}(f) & B_{re}(f) \\ A_{im}(f) & B_{im}(f) \end{vmatrix}$$

When T is given by:

$$T = \sqrt{A_{re}^{\ 2}(f) + A_{im}^{\ 2}(f) + B_{re}^{\ 2}(f) + B_{im}^{\ 2}(f)}$$

More explicitly:

$$S(f) = \frac{2\left[A_{re}(f)B_{im}(f) - A_{im}(f)B_{re}(f)\right]}{\sqrt{A_{re}{}^2(f) + A_{im}{}^2(f) + B_{re}{}^2(f) + B_{im}{}^2(f)}} \quad (4)$$

If the underground structure is 1D or 2D and environmental noise is zero, then the skew will be zero. Skew values below 0.2 are indicative of a 2D structure, skew values above 0.2 are an indication of 3D geology and/or higher noise levels.

3.1 Data analysis (preliminary considerations)

A Geomagnetic Deep Sounding analysis was performed for each of the three stations in the network array using sampled 1 Hz magnetic data. First the original data was filtered with a Butterworth filter (order 4) in the frequency band 1-450 mHz in order to eliminate the contribution of diurnal variation. The purpose was to investigate the electrical properties of the crust and upper mantle in the 1-100 Km range, and so this study used ULF signals of a skin depth (eq. 1) comparable to these values, considering a mean resistivity of $10^2\Omega$m. The upper limit of the frequency band chosen for the filter was the Nyquist frequency. Next, a survey was conducted for frequencies that satisfied the hypothesis of external field uniformity. This was achieved by searching for the 'spectral zone' where the coherence between the horizontal components calculated for each pair of magnetic stations is maximum (at least 0.8). Figure 9 shows an example (day 05 March 2015) of inter station coherence of the analogous magnetic components plotted against frequency. Coherence was calculated for all the possible pairs of magnetic stations. The vertical dotted lines indicate the limits of the applied 'selected' band: 10-50 mHz. This is the higher-frequency portion of the Pc4 and the lower-frequency portion of the Pc3 geomagnetic micropulsations band. These signals penetrate the Earth's interior down to distances of about 5-15 Km, which are the typical depths at which earthquakes hypocentres are located in the area investigated. They arise from electrical currents in the ionosphere excited by the magnetospheric Alfvén waves propagating along the geomagnetic field lines. They typically occur in daytime and are controlled by

various parameters like solar wind velocity, Interplanetary Magnetic Field intensity, and the cone angle value (Villante et al., 1992). Upstream waves driven by the solar wind through the magnetosphere are believed to be the principal mechanism responsible for the generation of Pc3-Pc4 micropulsations (Meloni et al. 2015). Figure 10 shows the mean daily values of the interstation coherence calculated in the 10-50 mHz frequency band from 2014 to May 2017. There is no data for 2013 because only the CLB station was working at the time. The lower coherence between the vertical components is due to different local inductive effects. Figures 11a, 11b, and 11c show the spectral amplitude ratio between the horizontal and vertical components calculated for three different frequency bands (1-10 mHz, 10-50 mHz, and 50-200 mHz) at CLB, PGN, and PRT, respectively. At lower frequencies, the horizontal components prevail over the vertical ones as foreseen on the basis of the sources cited above. The anomalous behaviour observed at the end of 2013 (at CLB, the only working station) seems to be caused by a greater influence of the Z component. Villante et al. (1998) conducted a long term (1985-1994) statistical analysis of man-made noise contamination in micropulsation measurements from the geomagnetic observatory of L'Aquila. They found a significant noise contribution to the local signal power in the 50-100 mHz band affecting mainly the X and Z components during weekdays (from Tuesday through Friday) with a minimum at weekends. Similar features are also observed at lower frequencies (5-45 mHz) with smaller weekly variations. A further analysis of magnetic measurements taken at the same site during a marked minimum in solar and magnetospheric activity (2008-2010) (Villante et al., 2014) revealed the existence of a persistent artificial signal that affects the natural daytime spectrum caused by a DC electrified railway located ~33 Km away from the L'Aquila geomagnetic observatory. The same characteristics are exhibited in the H and Z components above 50 mHz, while the D component is less explicitly affected and in a different manner. These studies suggest a possible influence of railway noise on the magnetic measurements taken at CLB at the end of 2013. An analysis of the coherence between each pair of magnetic components measured at CLB (fig. 12) shows that there is high coherence (~0.8) between H and Z. Moreover, the wave polarization characteristic (fig. 13) is well defined in this period. The wave vector was almost horizontal for many days, with a strong Z component contribution. The polarization analysis was achieved by calculating the amplitude and position of the pseudovector obtained from the spectral magnetic matrix. The first is proportional to the area of polarization ellipse, while the second corresponds to the wave vector direction. (Means J.D., 1972). The hypothesis of the influence of railways noise is

further supported by the analysis of the magnetospheric activity. Analysing the Kp index trend calculated at the Duronia geomagnetic observatory (fig. 14), a local minimum in magnetic activity can be observed at the end of 2013. Provided the railway traffic was not changed during this period, natural lower intensity signals allowed artificial noise to emerge.

3.2 Data analysis (results)

The real and imaginary parts of the induction arrow were evaluated minimizing the residual ε (eq. 2) relative to A and B by means of the standard least-squares method. (Everett and Hyndman, 1967, Gough and Ingham, 1983). They were calculated from the cross spectral densities as:

$$A(f) = \frac{< Z(f)X^*(f) >< Y(f)Y^*(f) > - < Z(f)Y^*(f) >< Y(f)X^*(f) >}{< X(f)X^*(f) >< Y(f)Y^*(f) > - < X(f)Y^*(f) >< Y(f)X^*(f) >}$$

$$B(f) = \frac{< Z(f)Y^*(f) >< X(f)X^*(f) > - < Z(f)X^*(f) >< X(f)Y^*(f) >}{< Y(f)Y^*(f) >< X(f)X^*(f) > - < Y(f)X^*(f) >< X(f)Y^*(f) >} \quad (5)$$

where the symbol < > indicates the mean values of cross spectra calculated over temporal sub intervals of equal length. The study applied a Hanning window of 512 seconds (frequency resolution is 2 mHz) covering the entire day without overlapping. Figures 15a, 15b, and 15c show the analysis for the three sites. The annual mean and standard deviation of both amplitude and phase are also reported. At CLB the real and imaginary tipper are almost parallel (~70°) except during periods of greater variation (real ~25° and imaginary ~40° at the end of 2013, real~90° and imaginary ~70° at the beginning of 2017). Their intensities are always comparable except at the end of 2013 when the amplitude of the real tipper prevails considerably over its imaginary part. Unlike 2013, the change observed during the spring of 2017 is only on the real tipper position. Furthermore, no corresponding greater influence of the Z component was observed, as seen from the spectral amplitude (fig. 11a) and polarization analysis (fig. 13) of the 10-50 mHz frequency band. The real tipper (amplitude and phase) appears to be most sensitive to changes involving its imaginary part. At PGN the tipper values were almost constant over the whole period. The real and imaginary tipper positions always differ by almost 30° (real ~70°, imaginary ~40°) and the amplitude is different, the real tipper always being slightly greater. Finally, at PRT no significant changes were observed in the real and imaginary parts for both amplitude and position (~70°). The data was more scattered compared to the other stations due to the greater artificial noise. To conclude, since the real

and imaginary induction arrows are approximately parallel for all three stations (lower subplot of figures. 15a, 15b, and 15c) the structure of the investigated area is dominated by a two-dimensional feature, with the induction arrows perpendicular to the conductivity contrast. Considering the position of the real tipper at ~70° for all the stations, it can be deduced that the area investigated is characterised by a geoelectric discontinuity (strike) along ~160° from magnetic North. This direction approximately coincides with the orientation (~140° from geographic North) of the fault system (Galadini F. And Galli P., 2000); (Vezzani L. and Ghisetti F., 1998) in the L'Aquila area. The flow of anomalous induced electric currents, due to horizontal magnetic field variations, in response to the electrical discontinuity, is parallel to the geoelectric strike. Finally, a further analysis of dimensionality was conducted by calculating the skew as defined by equation (4). The results are represented in figures 16a, 16b, and 16c. All the three stations exhibit 2D structures with different noise levels: for station PRT, skew mean value is slightly above 0.2, which may be due to higher artificial noise.

3.3 Discussion

The electrical properties of subsoil can be expressed by a simple RL circuit (resistance and inductance) (see appendix). The RL circuit model (fig. 17) can best represent the average properties of the EM response. The amplitude of the real (in-phase) and imaginary (out-of-phase) components of the EM response (TF) derive from the different sensitivity to the electrical characteristics, either reactive or resistive, of the conductors carrying the induced currents. In structures with electrical properties dominated by inductance rather than by resistance, the induced currents will be largely in-phase with the inducing fields, and so in this case the real part of the TF prevails. In structures in which resistance exceeds inductance, a considerable phase difference will occur between the induced and inducing fields, leading to a substantial imaginary part of TF accompanying the real part. The limit situations are represented by electric circuits whose impedance is totally inductive ($R\sim0$) or totally resistive ($\omega L\sim0$). The corresponding phase of the induced magnetic field, given by the equation in the Appendix, would become 0° in the first case and $\pi/2$ in the second case. However, the upper limit is not real because for low frequencies ($\sigma>>\omega\varepsilon$) the Earth's interior behaves as a good conductor ($\varphi \sim \pi/4$) but not as a super conductor ($\varphi\sim\pi/2$). So the expected angle varies between 0° (circuit completely inductive) and $\pi/4$ (circuit with resistance equal to inductance). Figure 18 shows the calculated phase shift between the induced (Z) and the

inducing (H and D) magnetic fields, related by equation (2). At CLB and PRT the subsoil presents a greater resistive component ($30° < \varphi < 60°$) than at PGN ($\varphi \sim 30°$). The CLB subsoil exhibits the greatest temporal variations in its electrical properties. According to the electrical model, the anomalous behaviour at the end of 2013 could be ascribed to a reduction in the electrical resistivity of the subsoil. This could explain the high inductive response at this time in the amplitude of the tipper, mainly in the real part (fig. 15a). On the other hand, this conclusion is in contradiction with the idea that at the end of 2013 the Z component of an artificial noise source prevailed over the magnetic measurements. This is because if resistivity reduces, the induced currents will oppose external signals (even noise) more strongly. These conclusions induce support for the idea that the anomalous behaviour of TF at CLB at the end of 2013 was due to a strong inductive response, rather than the presence of an external artificial noise that emerges from natural signals. According to the position of the real tipper arrows, this strong inductive response appears to be due to anomalous currents located at ~25° from magnetic North, maybe produced by the migration of a conductive fluid that could have modified the conductivity of the area under the CLB site. However, further analyses are required before this hypothesis can be confirmed. First of all, the nature of the vertical magnetic field observed at CLB at the end of 2013 needs to be better understood.

4 Conclusions

A long term (about four years, from 2013 to 2017) Geomagnetic Deep Sounding analysis was conducted in an area surrounding L'Aquila (central Italy), the city seriously damaged by the 6 April 2009 earthquake. One Hertz sampled data from an array of three magnetic stations (CLB, PGN, and PRT) were used for this purpose. The study was included within the framework of the Firb Abruzzo Project, a scientific project supported by the MIUR, aimed at investigating the Abruzzo area under different disciplinary approaches (geological, seismic, and physical). The inductive response of the subsoil to magnetic variations due to magnetospheric Pc3-Pc4 micropulsation sources (10-50 mHz) was analysed, computing the amplitude and position of the tipper arrow. The results revealed a 2D electrical structure for all three measurement sites. The real tipper, which is related to the inductive reactance of the subsoil, indicated a geoelectric discontinuity with an orientation of about ~160° relative to magnetic North. This orientation matches the typical fault disposition in the area investigated. The skew analysis confirmed the two dimensionality of the electrical structure. The real tipper

seems to be more sensitive to time variations than the imaginary part. According to a simple RL electrical circuit model, this implies that the inductive reactance of the subsoil is more susceptible to changes than the resistive reactance. At CLB and PRT the resistive component is greater than at PGN. PRT was seen to be the noisiest station. The major variation in inductive response observed at CLB at the end of 2013 was due to a reduction in the electrical resistivity of subsoil, probably caused by movement of some electrically charged fluid. According to the tipper position, the resulting anomalous electrical currents appear to be running at ~25° from magnetic North.

5 Appendix

The electrical RL model

A schematic representation is provided in figure 17.

The inducting magnetic field is given by:

$$B_{ext}(t) = B_0 e^{-j\omega t}$$

Where B_0 is the amplitude of the alternating magnetic induction field and ω is its angular frequency.

The induced electromotive force in the conductor is:

$$emf = -\frac{d\phi}{dt} = j\omega S B_0 e^{-j\omega t}$$

where S is the coil area. Thus, the current in the conductor is:

$$i(t) = \frac{j\omega S B_0 e^{-j\omega t}}{R + j\omega L}$$

The magnetic induction field corresponding to this current is:

$$B_{induced}(t) = c\frac{j\omega B_0 e^{-j\omega t}}{R + j\omega L}$$

Where the c parameter depends on several parameters, including the geometry of the conductor. Explicating:

$$B_{induced}(t) = -\frac{c\omega^2 L B_0 e^{-j\omega t}}{R^2 + \omega^2 L^2} + j\frac{c\omega R B_0 e^{-j\omega t}}{R^2 + \omega^2 L^2}$$

the phase shift between the induced and inducing field is

$$\phi = \tan^{-1}\frac{R}{\omega L}$$

For ωL>>R:

$$B_{induced}(t) \approx -c\frac{B_0 e^{-j\omega t}}{L}$$

$$\phi = \tan^{-1}\frac{R}{\omega L} \cong 0$$

so the inductive component gives an in-phase contribution relative to the inducing field B_0

For R >>ωL :

$$B_{induced}(t) \approx c\frac{j\omega B_0 e^{-j\omega t}}{R}$$

$$\phi = \tan^{-1}\frac{R}{\omega L} \cong \frac{\pi}{2}$$

the resistive component has a phase delay that approaches 90°.

Acknowledgements

This work was supported by the MIUR within the framework of the FIRB-Abruzzo project. We acknowledge the support of the technical staff at the Firb electromagnetic stations . We also thank the staff of the Duronia magnetic observatory for providing the geomagnetic Kp indices.

References

Alabi A.O.: *Magnetometer array studies*, Geophysical Surveys, 6, 153-172, 1983.

Anderson C.W., Lanzerotti L.J. and Maclennan C.G.: *Local Time Variation of Geomagnetic Induction Vectors*, Journal of Geophysical Research, Vo. 83, NO. B7, 1978.

Banks R.J. : *Data processing and interpretation in geomagnetic deep sounding*, Physics of the Earth and Planetary Interiors, 7, 339-348, 1973.

Brace W.F., Paulding B.W., J_R, Scholz C.: *Dilatancy in the Fracture of Crystalline Rocks*, Journal of Geophysical Research, Vol. 71, No.16, 1966.

Clifford G.D., *Singular Value Decomposition & Independent Component Analysis for Blind Source Separation*, Biomedical Signal and Image Processing Spring, 2005.

David A. Clark, New methods for interpretation of magnetic vector and gradient tensor data I: Eigenvector analysis and the normalised source strength, Exploration Geophysics, 2012

Di Lorenzo C., Pietrolungo M., Zirizzotti A., *Progetto FIRB-UR4 Installazione stazioni elettromagnetiche e validazione dei segnali registrati*, Rapporto Tecnico INGV. ISSN 2039-7941 N. 343, 2016.

Everett, J.E. and R.D. Hyndman: *Geomagnetic variation and electrical conductivity structure in South-western Australia*, Phys. Earth Planet. Inter., 1, 23-34, 1967.

Galadini F. and Galli P., *Active tectonics in the central Appennines (Italy) – input data for seismic hazard assessment*. Nat. Hazard, 22, 225-270, 2000.

Gubbins, D., Herrero-Bervera, E., *Encyclopedia of Geomagnetism and Paleomagnetism* Springer Editors: Gubbins, David, Herrero-Bervera, Emilio (Eds.) pags1054, 2007.

Gough D.Ian: *Magnetometer array studies, Earth structure, and tectonic processes*, Reviews of Geophysics, 27, 1/February, 1989.

Gough, D. I., and M. R. Ingham, *Interpretation methods for magnetometer arrays*, Rev. Geophys. 21, 805-827, 1983.

Hermance J.F.: *Electrical Conductivity Models of the Crust and Mantle*, Global Earth Physicsm 1995.

Means J.D.: *Use of the Three-Dimensional Covariance Matrix in Analyzing the Polarization Properties of Plane Waves*, Journal of Geophysical research, vol. 77, NO. 28, 1972.

Honkura Y., Matsushima M., Oshiman N., Tunçer M.K., Bariș Ș., Ito A., Iio Y., Ișikara A. M.: *Small electric and magnetic signals observed before the arrival of seismic wave*, Earth Planets Space, 54, e9-e12, 2002.

Hossein Hassani: *Singular Spectrum Analysis: Methodology and Comparison*, Journal of Data Science 5, 239-257, 2007.

Jones A.G.: *Geomagnetic Induction Studies in Scandinavia*, Journal of Geophysics, 48, 181-194, 1980.

Johnston M.J.S.: *Review of electric and magnetic fields accompanying seismic and volcanic activity*, Surveys in Geophysics, 18, 441-475, 1997.

Johnston M. J. S.: *Electromagnetic fields generated by earthquakes*, International Handbook of Earthquake and Engineering Seismology, part A, edited by: Lee, W., Kanamori, H., Jennings, P., and Kisslinger, K., 621–634, Academic Press, 2002.

Kharin E.P.: *Changes in transfer functions with time*, Geophysical Surveys, 4, 455-466, 1982.

Matsushita S.: *Solar quiet and lunar daily variation fields*, Physics of Geomagnetic Phenomena, 301-424, 1967.

Matsushita S., : *Sq and L current systems in the ionosphere*, Geophys. J. R. Astron. Soc., 15, 109-125, 1968.

McPherron, R. L., C. T. Russel, and P.J. Coleman Jg., *Fluctuating Magnetic Fields in the Magnetosphere*, Space Science Reviews 13 411—454,1972.

A Meloni, C Bianchi, G Mele, P Palangio. *Background electromagnetic noise characterization: the role of external and internal Earth sources*, Annals of Geophysics 58 (3), G0330, 2015.

Means J.D.: *Use of the Three-Dimensional Covariance Matrix in Analyzing the Polarization Properties of Plane Waves*, Journal of Geophysical research, vol. 77, NO. 28, 1972.

Molchanov O.A. and Hayakawa M.: *Generation of ULF electromagnetic emissions by microfracturing*, Geophysical Research Letters, Vol. 22, No.22, 3091-3094, 1995.

Molchnanov O.A. and Hayakawa M., On the generation mechanism of ULF seismogenic electromagnetic emissions, Physics of the Earth and Planetary Interiors 105, 201-210, 1998

Naidu G. D., *Deep Crustal Structure of the Son-Narmada-Tapti Lineament, Central India*, Springer Theses, 2012.

Niblett E.R.: *Time-dependence of electromagnetic transfer functions and their association with tectonic activity*, Geophysical Surveys, 4, 97-114, 1980.

Palangio P., Masci F., Di Lorenzo C. and Di Persio M.: *The wideband [0.001 Hz–100 kHz] interferometry project in Central Italyt*, Geophysical Prospecting, 57, 729-737, 2009.

Pinçon J.L., Menvielle M., Szarka L.: *Geomagnetic induction study using the NetLander network of magnetometers*, Planetary and Space Science 48, 1261-1270, 2000.

Rowlands G. and Sprott J.C.: *Extraction of dynamical equations from chaotic data*, Physica D 58 251-259, 1992.

Saito S., Kaida D., Hattori K., Febriani F. and Yoshino C.: *Signal discrimination of ULF electromagnetic data with using singular spectrum analysis – an attempt to detect train noise*, Nat. Hazards Earth Syst. Sci., 11, 1863-1874, 2011.

Scholz C.H., Sykes L.R. and Aggarwal Y.P.: *Earthquake Prediction: A Physical Basis*, Science, 181, 803-810, 1973.

Schmucker U.: *An Introduction to Induction Anomalies*, Journal of Geomagnetism and Geoelectricity, Vol. 22, No.1-2,1970.

Schmucker U.: *REGIONAL INDUCTION STUDIES: A REVIEW OF METHODS AND RESULTS*, Physics of the Earth and Planetary Interiors, 7, 365-378,1973.

Surkov V.V. and Pilipenko V.A.: *Magnetic effects due to earthquakes and underground explotions: a review*, Annali di Geofisica, Vol. XL, N.2, March 1997.

Ujihara N., Honkura Y. and Ogawa Y.: *Electric and magnetic field variations arising from the seismic dynamo effect for aftershocks of the M7.1 earthquake of 26 May 2003 off Miyagi Prefecture*, NE Japan, Earth Planets Space, 56, 115-123, 2004.

Vezzani L. and Ghisetti F.; *Carta Geologica dell'Abruzzo*. S.EL.CA., Firenze, 1998.

Villante U. and Vellante M.: *An analysis of working days contamination in micropulsation measurements*, Annali di Geofisica, Vol. 41, N.3, August 1998.

Villante U., Lepidi S., Vellante M., Lazarus A.J. and Lepping R.P.: *Pc3 activity at low geomagnetic latitudes: a comparison with solar wind observations*, Planetary Space Science, 40, 1399, 1992.

Villante U., Piancatelli A. and Palangio P., *On the man-made contamination on ULF measurements: evidence for disturbances related to an electrified DC railway*, Annales Geophysicae, 32, 1153-1161, 2014.

McPHERRON, R. L., C. T. RUSSELL, and P.J. COLEMAN Jg., *Fluctuating Magnetic Fields in the Magnetosphere*, Space Science Reviews 13 411—454,1972

(Geomagnetic Deep Sounding and Upper Mantle Structure in the Western United States J. S. Reitzel,)

Figure 1. The interferometric array.

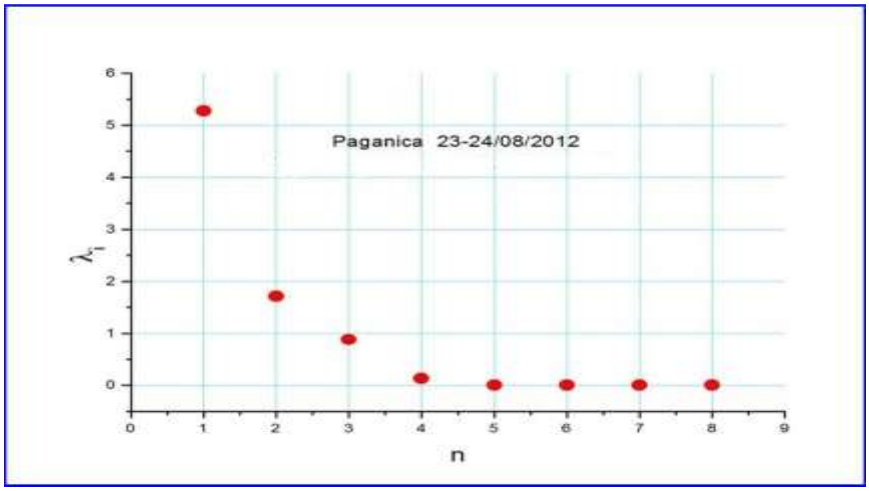

Figure 2. The first eight eigenvalues of the covariance matrix.

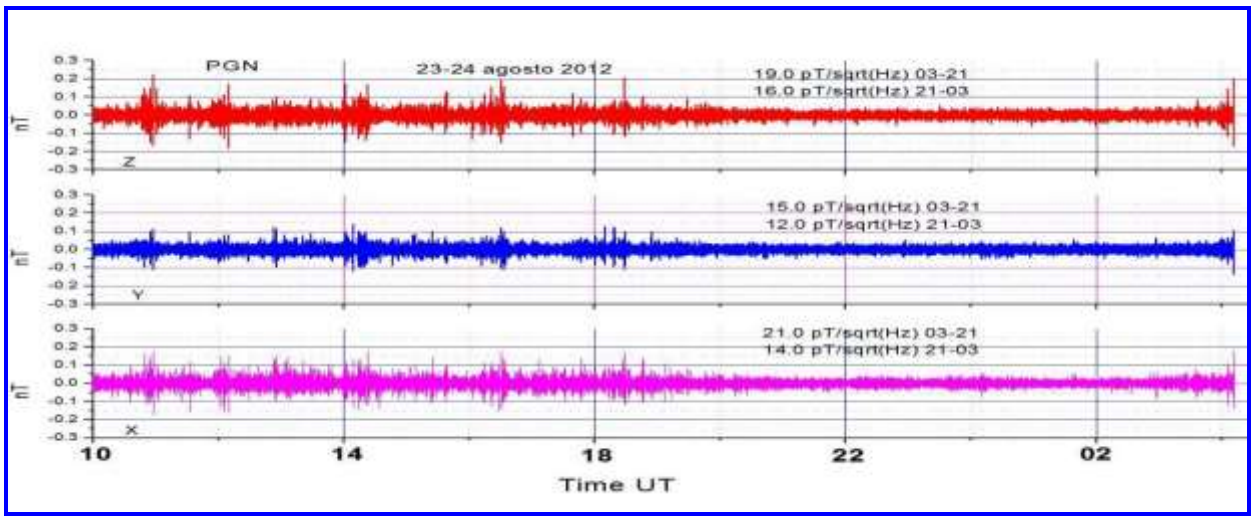

Figure 3. Noise at PGN.

Figure 4. The CLB site.

Figure 5. The PGN site.

Figure 6. The PRT site.

Figure 7. Search coil magnetometer sensors.

Figure 8. Flux gate magnetometer sensors.

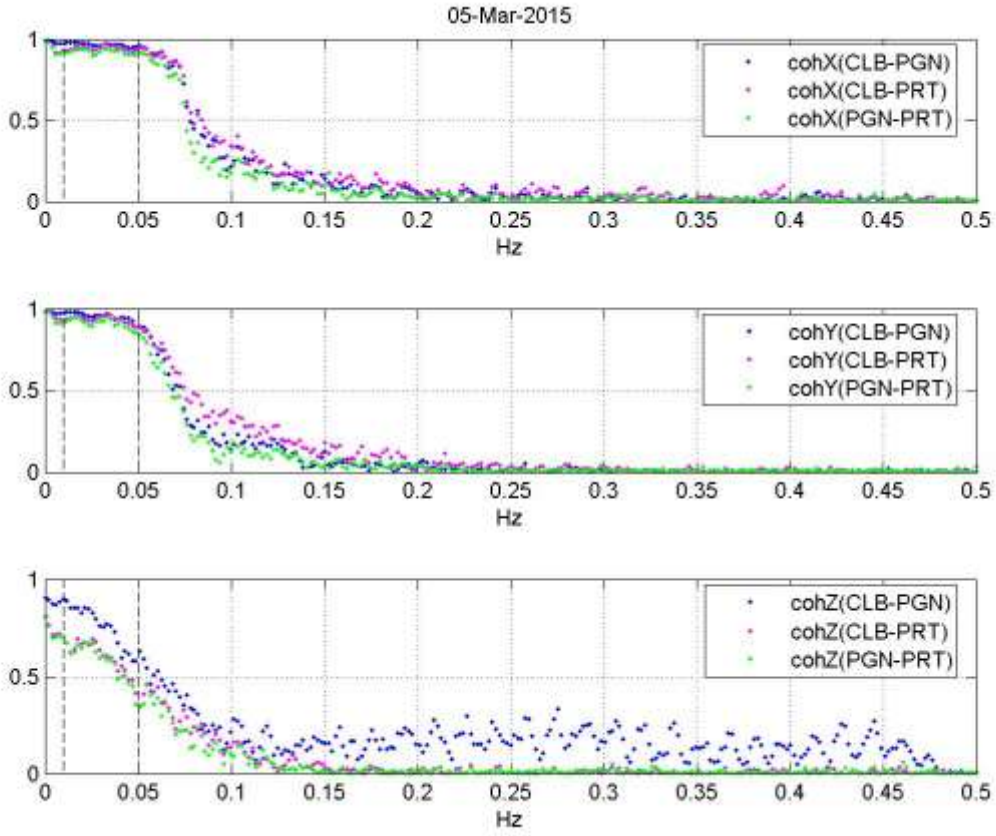

Figure 9. An example of interstation coherence between the analogous magnetic components plotted against frequency. The vertical dotted lines indicate the chosen frequency band limits where the coherence between horizontals components is maximum.

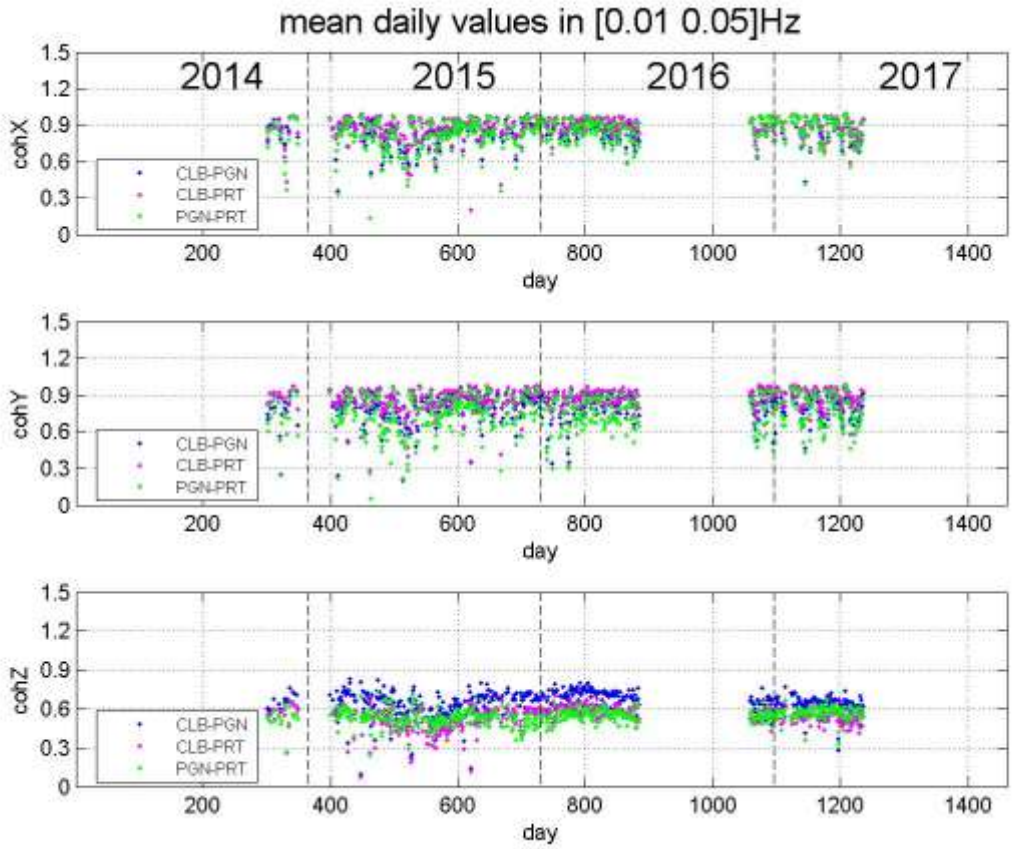

484

485 Figure 10. Mean daily values of interstation coherence between analogous magnetic field
486 components calculated in the 10-50 mHz frequency band.

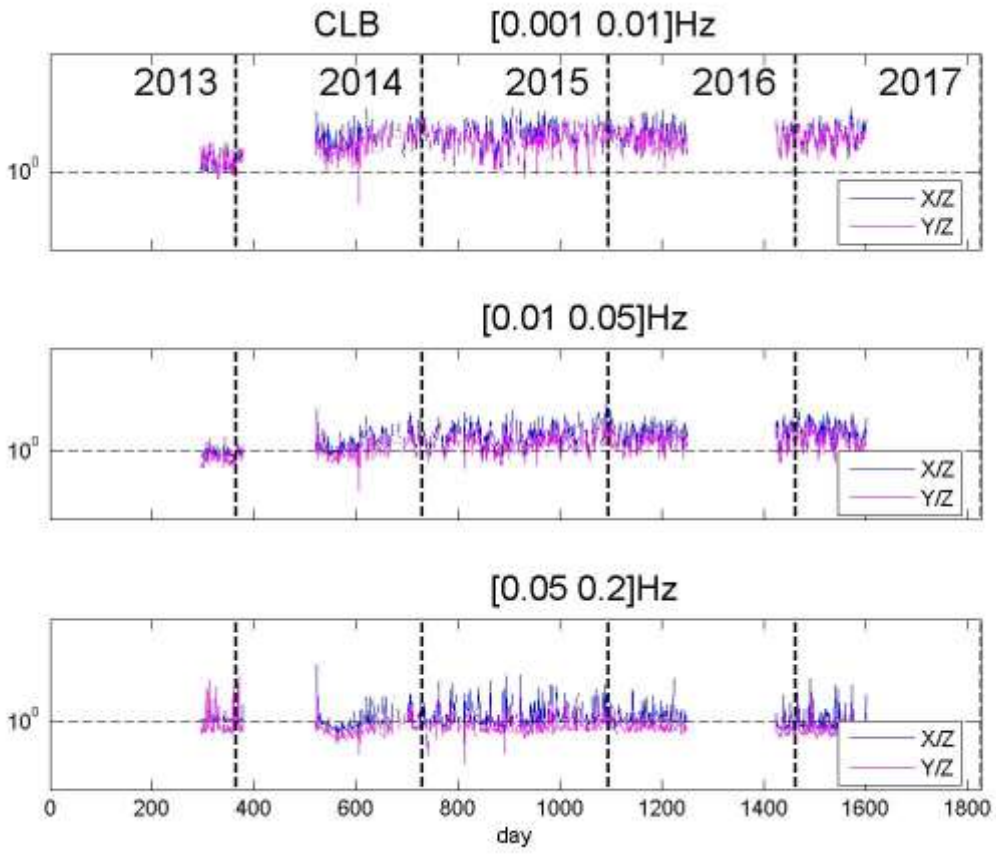

487

488 Figure 11a. Spectral amplitude ratio between horizontal and vertical components at the CLB
489 station, calculated for three different frequency bands.

490

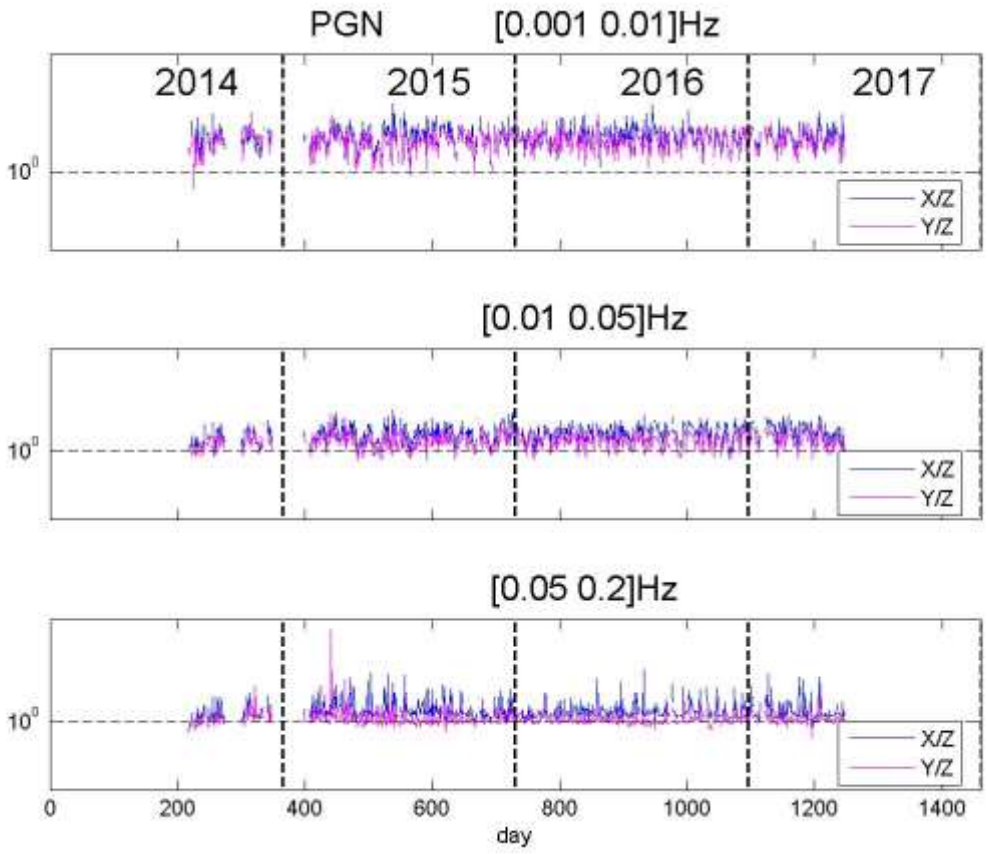

491

492 Figure 11b. Spectral amplitude ratio between horizontal and vertical components at the PGN
493 station, calculated for three different frequency bands.

494

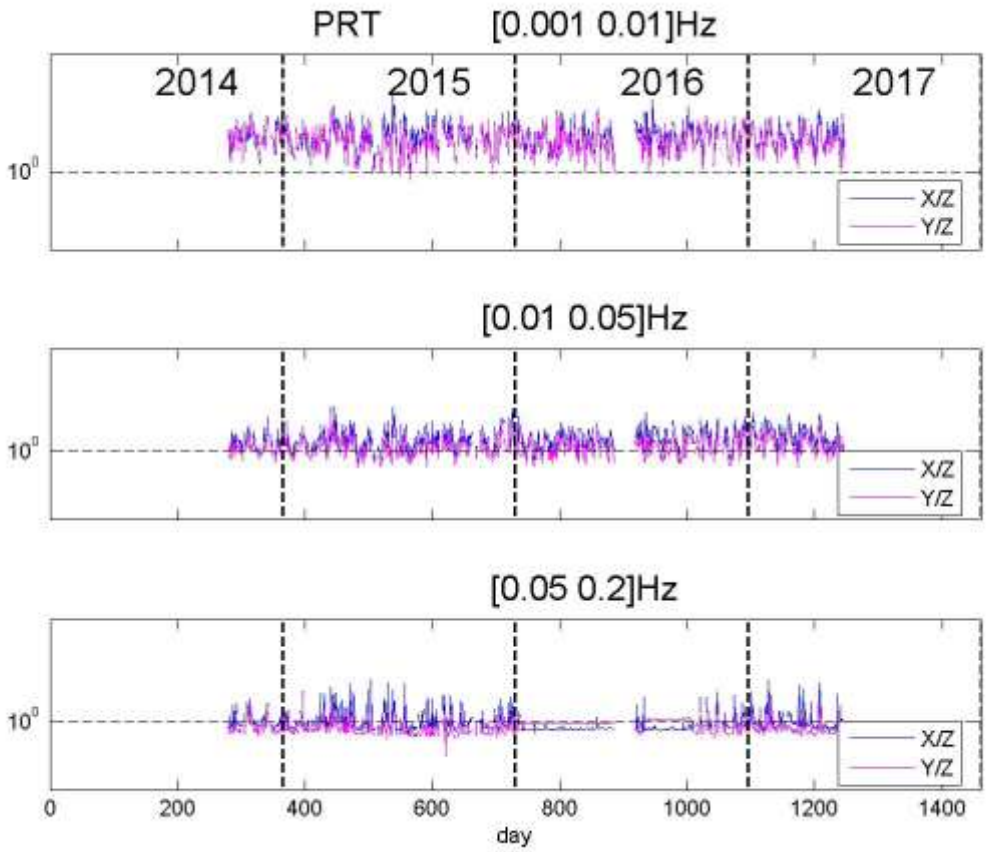

495

496 Figure 11c. Spectral amplitude ratio between horizontal and vertical components at the PRT
497 station, calculated for three different frequency bands.

498

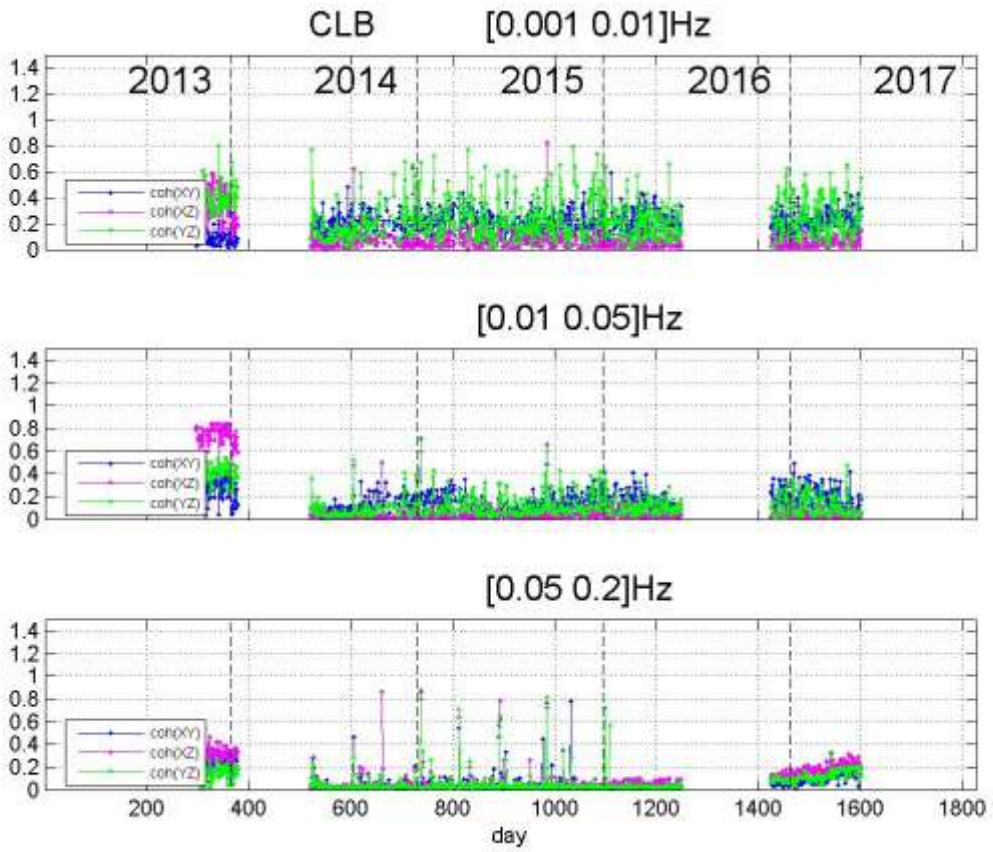

Figure 12. Coherence between magnetic components at CLB calculated for the same frequency bands of figures 11a, 11b, and 11c. At the end of 2013 and at the beginning of 2014 the [0.01 0.05] Hz band was characterised by the highest coherence between X and Z.

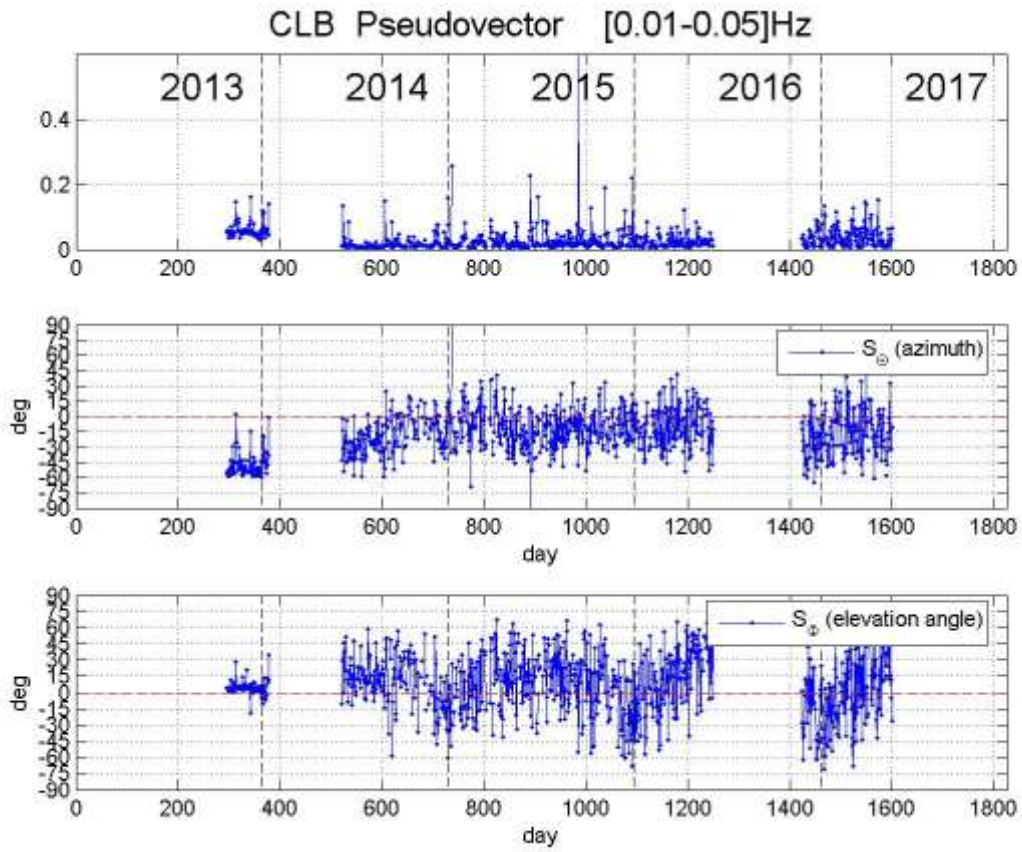

505
506 Figure 13. The magnetic signal polarization study at the CLB station.

507

508

509

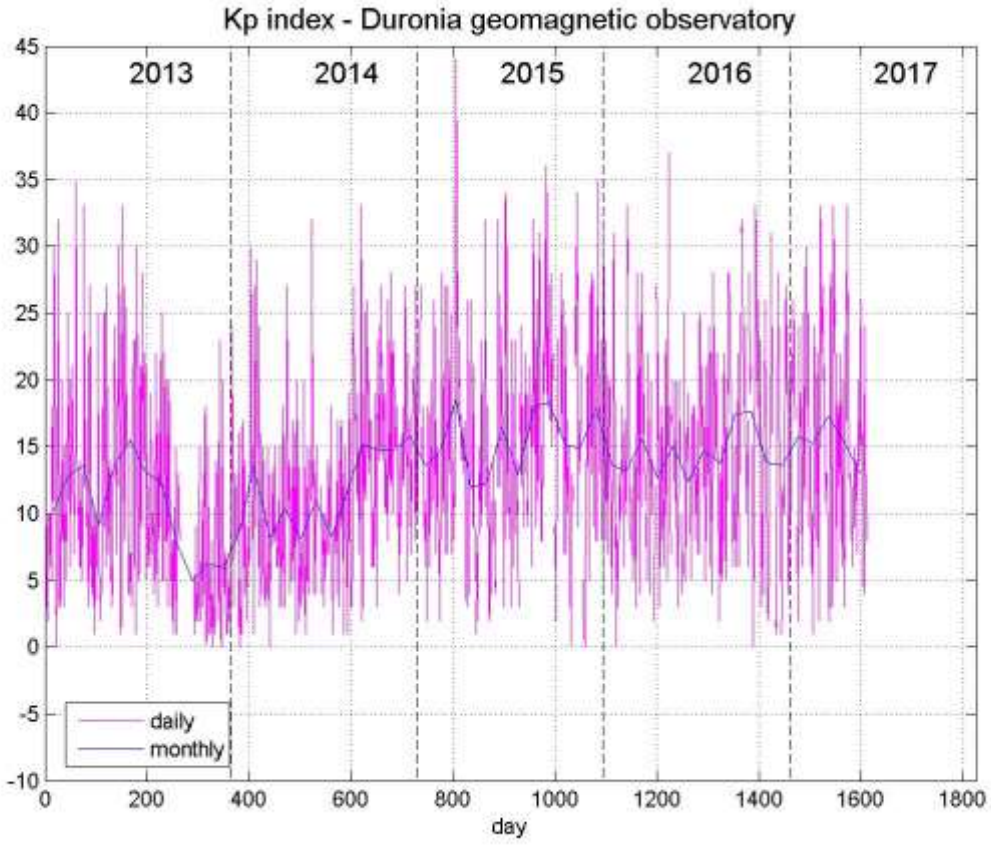

510
511 Figure 14. The Kp index calculated at the Duronia geomagnetic observatory.

512

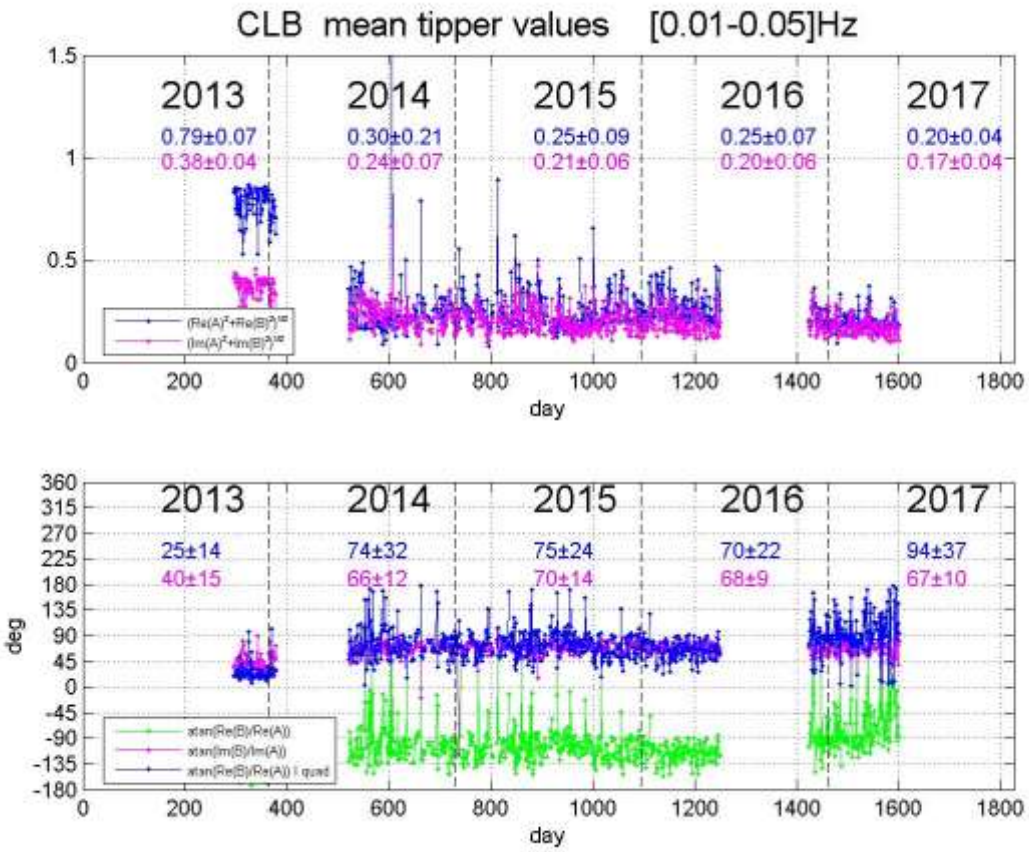

513

514 Figure 15a. Mean daily values of magnitude and phase of induction arrow at CLB, calculated
515 in the [0.01 0.05] Hz frequency band. (Data filtered over the whole [0.001 0.45] Hz band
516 were used.)

517

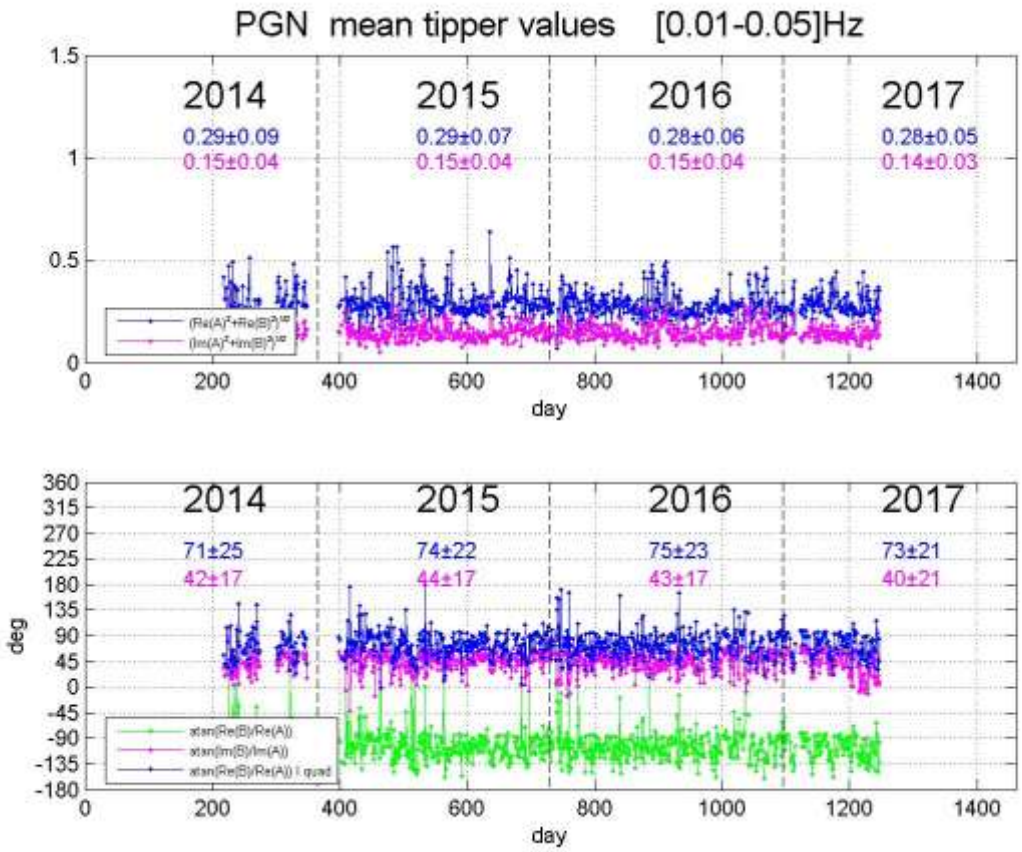

518

519 Figure 15b. Mean daily values of magnitude and phase of induction arrow at PGN, calculated
520 in the [0.01 0.05] Hz frequency band. (Data filtered over the whole [0.001 0.45] Hz band
521 were used.)

522

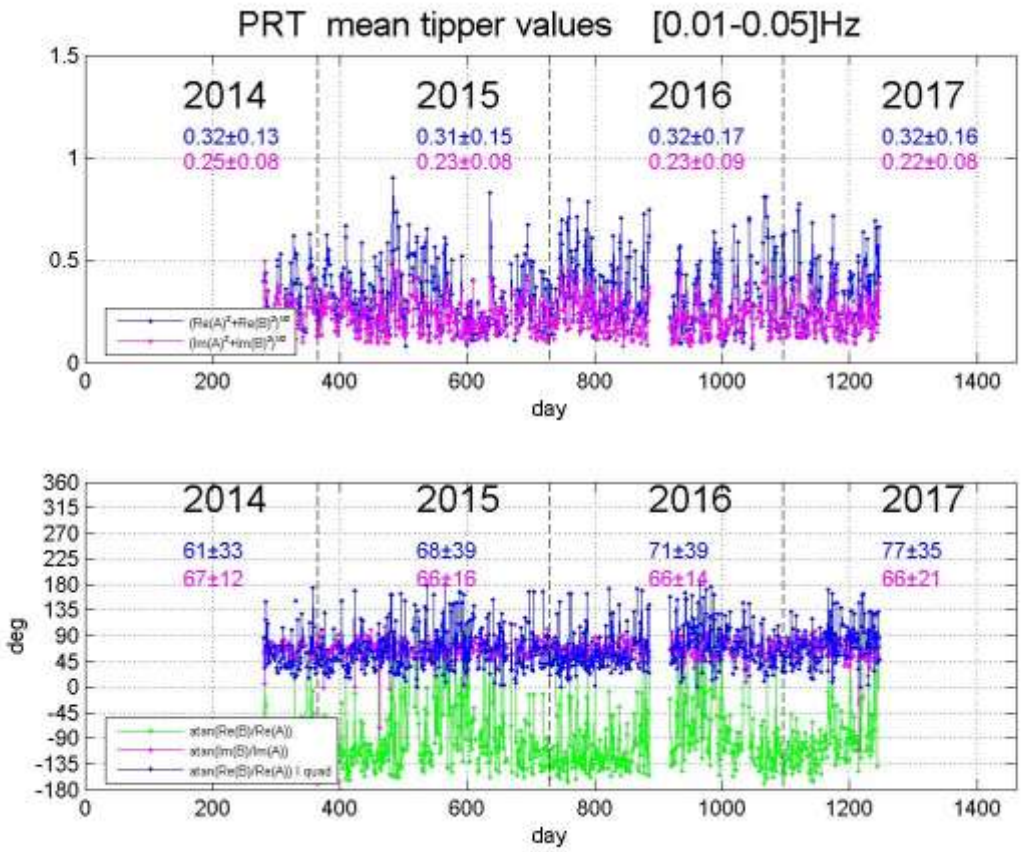

523

524 Figure 15c. Mean daily values of magnitude and phase of induction arrow at PRT, calculated
525 in the [0.01 0.05] Hz frequency band. (Data filtered over the whole [0.001 0.45] Hz band
526 were used.)

527

528

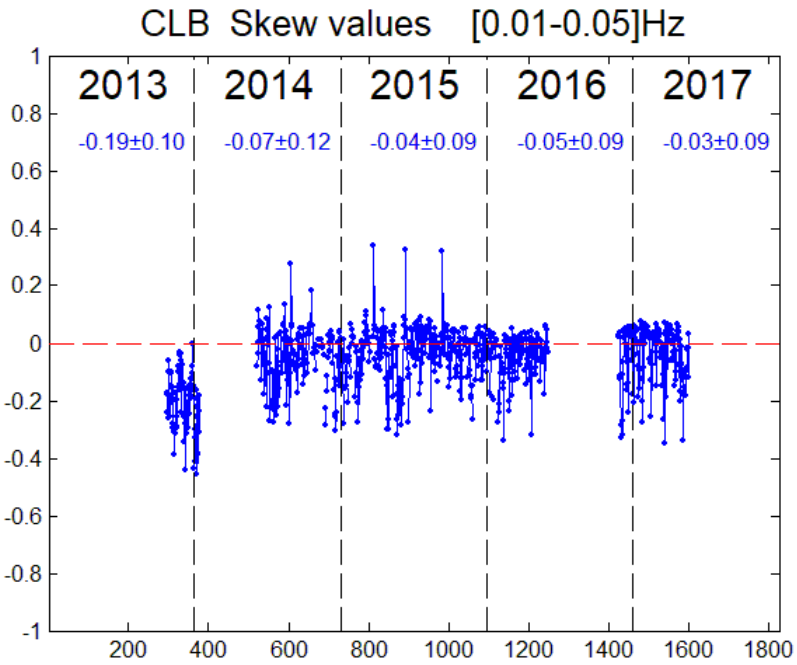

529

530 Figure 16a. The tipper skew at CLB.

531

532

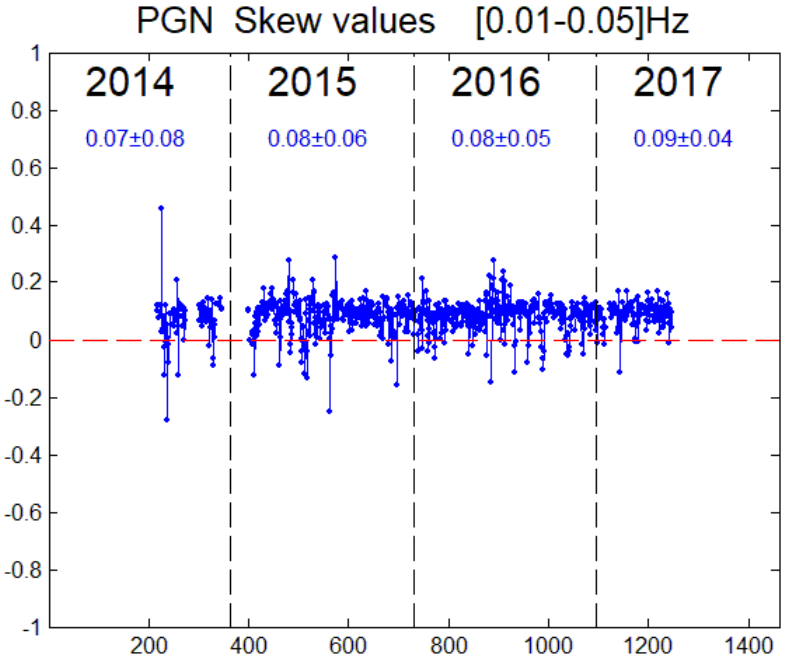

533

534 Figure 16b. The tipper skew at PGN.

535

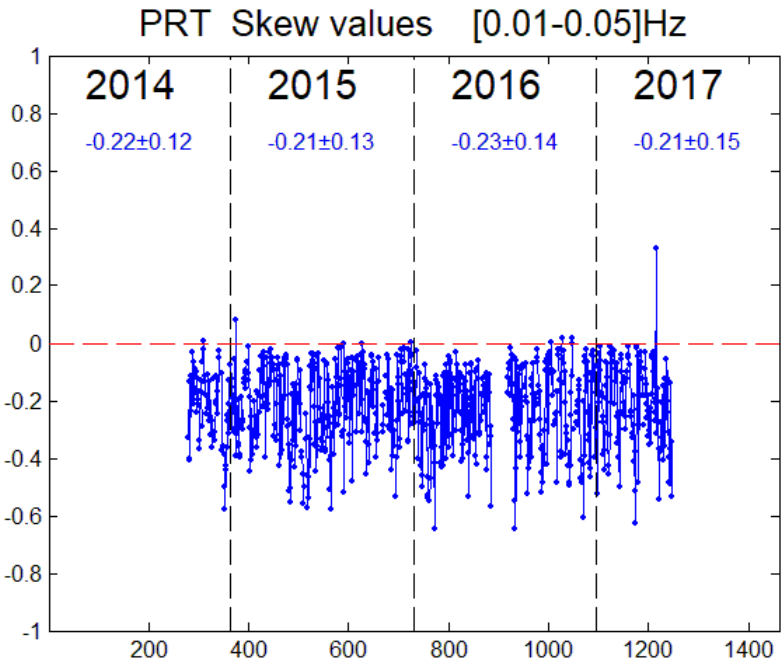

536

537

538

539

540 Figure 16c. The tipper skew at PRT.

541

542

543

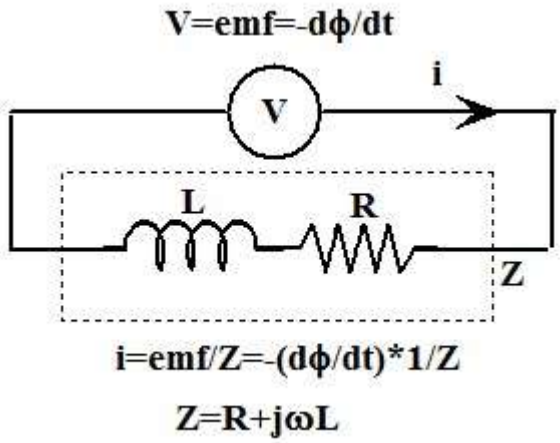

544

545 Figure 17. Schematic electrical model of subsoil.

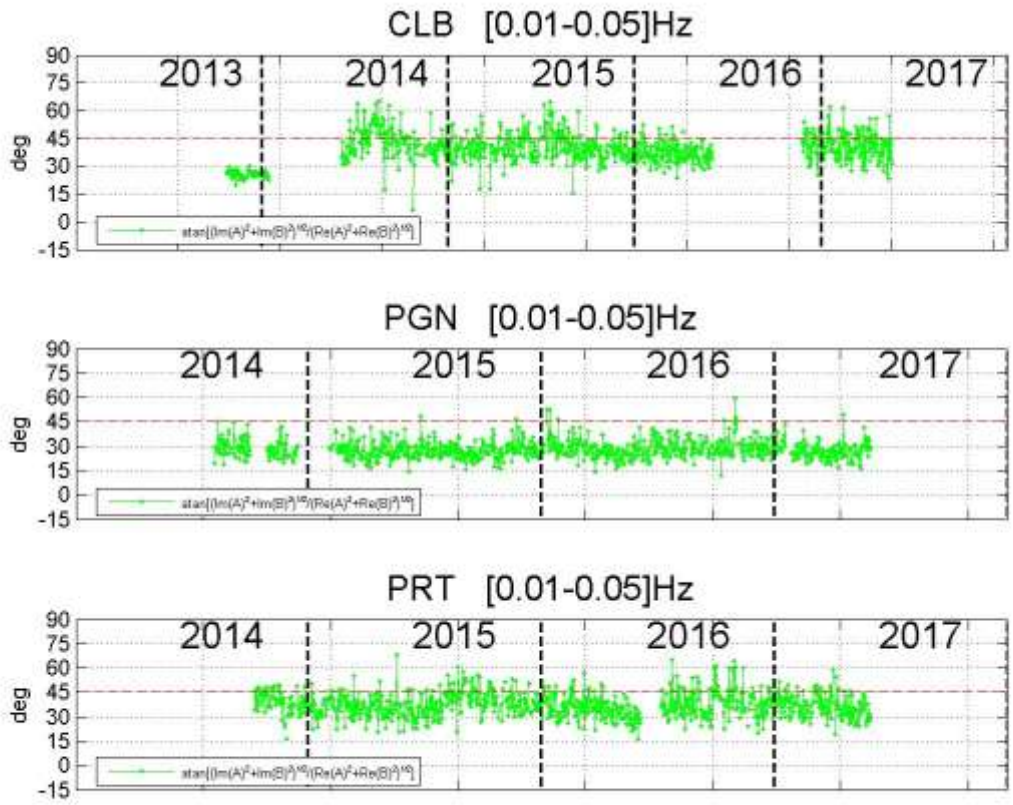

546

547 Figure 18. The phase between the induced vertical component (Z) and the inducing horizontal
548 components (H and D).